Journal of Sound and Vibration (2000) **231**(5), 1355–1376
doi:10.1006/jsvi.1999.2738, available online at http://www.idealibrary.com on IDEAL®

NON-STATIONARY FUNCTIONAL SERIES TARMA VIBRATION MODELLING AND ANALYSIS IN A PLANAR MANIPULATOR

K. A. PETSOUNIS AND S. D. FASSOIS

Stochastic Mechanical Systems (SMS) Group, Department of Mechanical & Aeronautical Engineering, University of Patras, GR 265 00 Patras, Greece

(*Received* 2 *March* 1999, *and in final form* 26 *October* 1999)

The problem of non-stationary stochastic vibration modelling and analysis is considered through a paradigm involving vibration analysis in a periodically varying manipulator. A parametric Functional Series method based upon time-dependent autoregressive moving average (TARMA) models is applied for the first time within the vibration analysis context, and comparisons with both pure TAR and non-parametric Fourier-based analysis are made. These focus on achievable time-dependent spectrum accuracy, resolution, and tracking, as well as on estimated modal parameter accuracy. The Functional Series TARMA method is shown to lead unambiguously to a physically meaningful $\text{TARMA}(4, 5)_{p=3}$ representation, while the pure TAR method leads to a $\text{TAR}(12)_{p=3}$ representation. The $\text{TARMA}(4, 5)_{p=3}$ model is shown to achieve superior spectral and modal parameter accuracy, while avoiding the problem of estimated false modal modes of its $\text{TAR}(12)_{p=3}$ counterpart. The $\text{TARMA}(4, 5)_{p=3}$ model also attains lower parametric complexity and superior values of the model fit criteria. The study demonstrates the facets and capabilities of the Functional Series TARMA method for non-stationary vibration analysis, indicating that the TARMA model's direct relationship with the underlying physical system constitutes an important asset of the method.

1. INTRODUCTION

Non-stationary signals are characterized by features that vary with time and require time–frequency methods for their analysis [1, 2]. Such signals occur in systems with time-dependent properties and/or non-linearities. Notable examples of non-stationary vibration include traffic-excited bridge vibration, earthquake-excited vibration, vibration in surface vehicles, airborne structures and sea vessels, in robotic devices, rotating machinery, and so on. Due to the large number and variety of non-stationary vibration signals, time–frequency analysis methods have been receiving increasing attention in recent years [2].

A classical, as well as largely empirical, time–frequency analysis tool has been the short-time fourier transform (STFM) and its ramifications [2]. Other *non-parametric methods* include Priestley's evolutionary spectrum [3], Wigner–Ville distributions and their extensions [1], as well as wavelet-based methods [4, 5].

0022-460X/00/151355 + 22 $35.00/0

Although offering advantages such as representation parsimony, improved-accuracy, resolution, and tracking, as well as flexibility in analysis, synthesis, prediction, and control, *parametric methods* have received considerably less attention and are scarcely used in non-stationary vibration analysis. Among them, *adaptive methods* [6, 7], based upon recursive estimation schemes, are appropriate for slowly varying signals and involve a trade-off between tracking ability and achievable accuracy. *Stochastic parameter evolution methods*, postulating signal representations with time-dependent coefficients obeying stochastic smoothness constraints [8], impose additional "structure" on parameter evolution, which may, nevertheless, be still insufficient in certain applications. This may be due to the fact that the underlying physical mechanisms responsible for the non-stationary behaviour change in a more systematic (deterministically organized) way. Such an evolution may be often best captured by *functional series methods* [9, 10], which postulate signal representations with parameters belonging to a functional subspace. These methods thus impose further "structure" on parameter evolution, achieving a high degree of parsimony and the capability of tracking fast and abrupt changes while maintaining high accuracy and resolution.

The *thesis* upon which this work is based is that, in spite of the minimal attention that it has received, the Functional Series approach is both physically motivated and applicable for non-stationary vibration analysis. The *goal* of the study thus is to demonstrate its applicability and to explore its effectiveness in both modelling and analysis through a manipulator vibration paradigm.

The manipulator vibration paradigm considered concerns the non-stationary modelling and analysis of random vibration in a two-link planar manipulator. The manipulator vibration is due to the stationary random component of an externally applied torque. Although the system is assumed to operate in a linearized regime, around a nominal position, the vibration is non-stationary due to the system's time-varying configuration stemming from the motion of two ring-type masses along the manipulator links (section 2.1). This makes it a notable non-stationary system characterized by time-dependent properties.

The functional series method used in the study is based upon non-stationary time-dependent autoregressive moving average (TARMA) modelling. TARMA models are conceptual extensions of their conventional (stationary) ARMA counterparts, in that their parameters are explicit functions of time [9, 10] (see section 3.1). Depending upon the form of these functions, TARMA models are capable of representing either smooth or abrupt spectral evolution, and thus making the Functional Series TARMA method applicable to a wide range of non-stationary signals. Yet, with very few exceptions that have been limited to the pure TAR case [11], functional series TARMA models have not been previously used in non-stationary vibration signal analysis.

The study thus focuses, for the first time, on the Functional Series TARMA method's facets and capabilities for vibration signal modelling and analysis. Particular emphasis is placed on the achievable time-dependent spectrum accuracy, resolution, and tracking, as well as on the estimated modal characteristics. Within this context, the suitability and discriminating power of model selection criteria, such as the residual sum of squares (RSS) and Akaike's first and second

information criteria (AIC/BIC) [8], are examined. Finally, enlightening comparisons with the pure TAR and non-parametric Fourier-based spectral estimation are performed, and certain advantages of the mixed TARMA method — and the general Functional Series approach — are discussed.

The rest of this paper is organized as follows. The manipulator non-stationary vibration, along with its theoretical characteristics and simulation, are discussed in section 2. The vibration signal Functional Series TARMA modelling is presented in section 3, whereas model validation and analysis — including comparisons with TAR and non-parametric Blackman–Tukey-type Fourier-based analysis — are discussed in section 4. The conclusions of this study are summarized in section 5.

2. MANIPULATOR NON-STATIONARY VIBRATION

2.1. SYSTEM DESCRIPTION

The two-link planar manipulator used in the study is depicted in Figure 1. Each link is considered to be a rigid, uniform, cylinder of length l and mass m. The first link is connected to the base by means of an elastic spring-hinge of torsional stiffness k_1, while the second is connected to the first by a similar spring of stiffness k_2. A ring-type mass is allowed to move along each link; the instantaneous distance of the first one (μ_1) from the base joint is designated as r_1, and that of the second

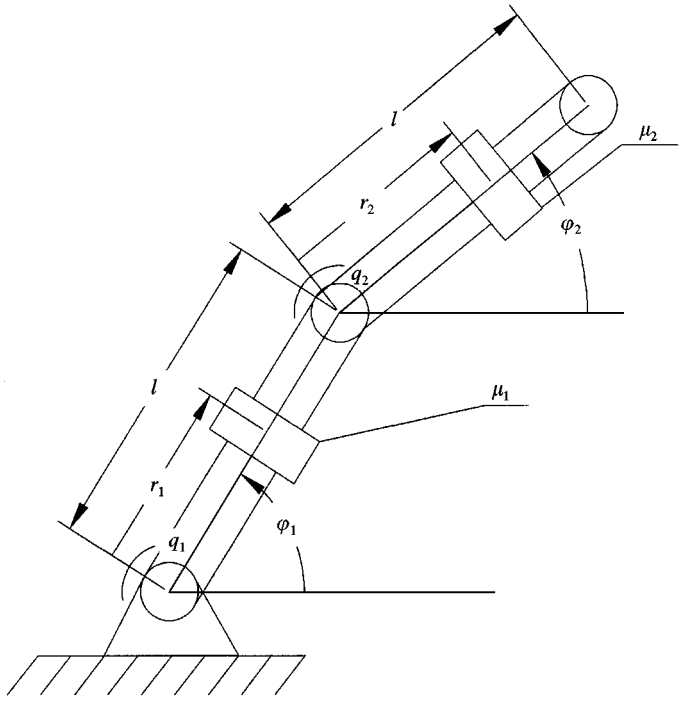

Figure 1. Schematic diagram of the two-link planar manipulator.

(μ_2) from the second joint is designated as r_2. Such manipulators are considered in Reference [12]. Let q_1, q_2 designate external torques applied at the joints, and ϕ_1, ϕ_2 the link angular positions with respect to the positive horizontal axis (Figure 1).

The manipulator is assumed to operate around a nominal position (ϕ_{10}, ϕ_{20}). The actual link positions are then expressed as $\phi_1 = \phi_{10} + \phi_{11}$ and $\phi_2 = \phi_{20} + \phi_{21}$, with ϕ_{11}, ϕ_{21} designating the link angular displacements relative to their nominal positions. Under a small angular displacement assumption, a linearized model of the system around the nominal position is (bold face lower-case/capital characters designate vector/matrix quantities, respectively)

$$\mathbf{M}(t)\cdot\ddot{\boldsymbol{\phi}} + \mathbf{D}(t)\cdot\dot{\boldsymbol{\phi}} + \mathbf{K}\cdot\boldsymbol{\phi} = \mathbf{q}(t), \tag{1}$$

with t indicating continuous time, $\boldsymbol{\phi} = [\phi_{11}\ \phi_{21}]^{\mathrm{T}}$ the (relative) angular displacement vector (in radians), and $\mathbf{M}(t)$, $\mathbf{D}(t)$, $\mathbf{K}$ the mass, damping, and stiffness matrices which are of the forms

$$\mathbf{M}(t) = \begin{bmatrix} \alpha_1 + \mu_1 r_1^2 + \mu_2 l^2 & (\alpha_2 + \mu_2 r_2 l)\cos(\delta\phi_0) \\ (\alpha_2 + \mu_2 r_2 l)\cos(\delta\phi_0) & \alpha_3 + \mu_2 r_2^2 \end{bmatrix}, \tag{2}$$

$$\mathbf{D}(t) = \begin{bmatrix} 2\mu_1 r_1 \dot{r}_1 & \mu_2 \dot{r}_2 l\cos(\delta\phi_0) \\ \mu_2 \dot{r}_2 l\cos(\delta\phi_0) & 2\mu_2 r_2 \dot{r}_2 \end{bmatrix} + a\cdot\mathbf{K}, \tag{3}$$

$$\mathbf{K} = \begin{bmatrix} k_1 + k_2 & -k_2 \\ -k_2 & k_2 \end{bmatrix}, \tag{4}$$

with $\dot{r}_i$ indicating time derivative of r_i. The input vector is of the form

$$\mathbf{q}(t) = \begin{bmatrix} q_1(t) - q_2(t) \\ q_2(t) \end{bmatrix} \tag{5}$$

while $\alpha_1 \triangleq 4ml^2/3$, $\alpha_2 \triangleq ml^2/2$, $\alpha_3 \triangleq ml^2/3$, $\delta\phi_0 \triangleq \phi_{10} - \phi_{20}$. Notice that the damping matrix [equation (3)] includes an extra proportional damping term, with a representing the coefficient of proportionality. The numerical values of the system parameters are indicated in Table 1.

2.2. THEORETICAL SIGNAL CHARACTERISTICS

The manipulator vibration around the nominal position $(\phi_{10}, \phi_{20}) = (45^\circ, 0^\circ)$ and under a broadband (uncorrelated) stationary unobservable torque excitation $q_1(t)$ (correlated excitations could be also used; their characteristics would then have to be incorporated in the vibration response TARMA model) is considered,

TABLE 1

System parameters

Property	Symbol	Value
Length of links 1 and 2	l	1 m
Mass of links 1 and 2	m	1 kg
Sliding ring-type masses	μ_1, μ_2	0·25 kg
Stiffness of torsional spring 1	k_1	100 Nm/rad
Stiffness of torsional spring 2	k_2	80 Nm/rad
Proportional damping coefficient	a	0·005

whereas $q_2(t) \equiv 0$. The sliding ring-type masses μ_1, μ_2 move along their respective links following sinusoidal trajectories of the form

$$r_i(t) = r_{i0} + \delta r_i \cdot \sin(2\pi t/P), \quad i = 1, 2 \tag{6}$$

with $P = 2$ s indicating the motion period, $r_{i0} = 0{\cdot}5$ m, and $\delta r_i = 0{\cdot}3$ m ($i = 1, 2$). The system response of interest is the vibration displacement ϕ_{21} of the second link.

Due to the periodic motion of the ring-type masses, the system is (periodically) non-stationary with period $P = 2$ s (corresponding frequency $f_p = 0{\cdot}5$ Hz), henceforth referred to as the *system period*. The theoretical time-dependent spectrum ("frozen" spectrum [9]) of the ϕ_{21} vibration signal under stationary uncorrelated excitation $q_1(t)$, and computed via the system equation (1) by multiplying the torque excitation spectrum with the magnitude squared of the frequency response function $\phi_{21}(j\omega)/q_1(j\omega)$ [5], j designating the imaginary unit and ω frequency, is presented (in both 3-D and contour plots) in Figure 2 as a function of time and frequency. The following remarks may be made from this continuous-time spectrum.

(a) The theoretical time-dependent spectrum is, expectedly, periodic, with the exact same period as the system ($P = 2$ s).
(b) The signal's main energy concentration is in the 0–6 Hz frequency band. Its two natural frequencies $f_1(t)$ and $f_2(t)$, varying in the (0·84, 0·92) and (3·48, 3·90) Hz ranges, respectively, are separated by a spectral valley. The $f_1(t)$ frequency is dominant, while the system is lightly damped with each damping ratio trajectory being bounded by 0·07.

2.3. SIGNAL SIMULATION

Based upon the previous remarks, the torque excitation $q_1(t)$ is selected as a zero-mean low-pass filtered (cut-off frequency $f_c = 6$ Hz) uncorrelated signal

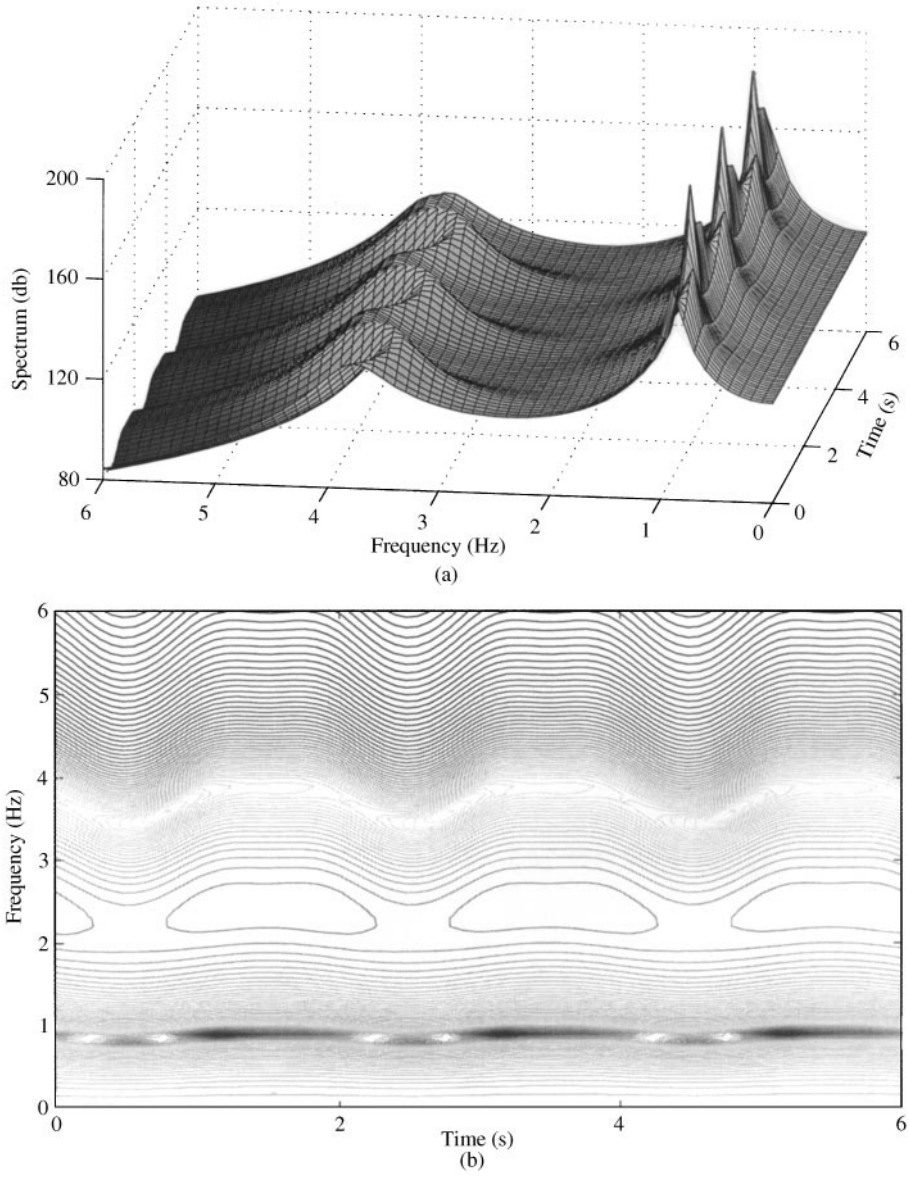

Figure 2. Theoretical time-dependent spectrum of the signal (continuous-time). (a) 3-D plot; (b) contour plot.

sampled at 25 Hz. The system equation is integrated by using a Runge–Kutta 4/5 method with variable integration step, and the generated vibration response is also low-pass filtered ($f_c = 6$ Hz) and re-sampled at $f_s = 12{\cdot}5$ Hz. To minimize transient effects, an initial segment of the resulting signal is dropped, with the remaining signal being $\Delta T = 236$ s or 2950 samples long. An important observation to be made at this point is that the number of signal samples per system period is only $N_p = 25$.

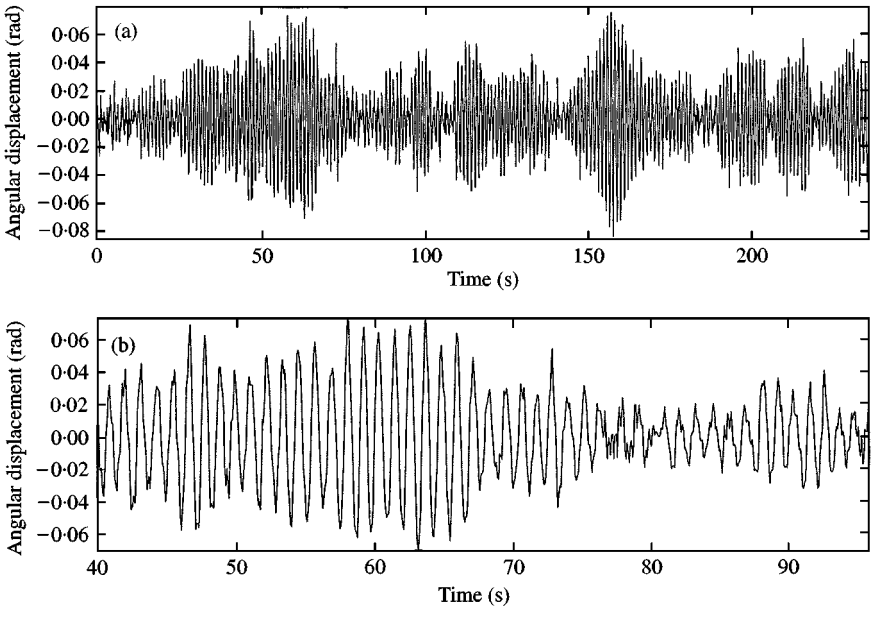

Figure 3. The vibration displacement signal modelled ($f_s = 12{\cdot}5$ Hz). (a) Complete signal record; (b) signal portion.

The signal is depicted in Figure 3, from which its non-stationary behaviour is evident. In agreement with previous remarks, a closer examination reveals the domination of the $f_1(t)$ frequency.

3. FUNCTIONAL SERIES NON-STATIONARY VIBRATION SIGNAL MODELLING

3.1. THE FUNCTIONAL SERIES TARMA METHOD

The Functional Series TARMA method advocates non-stationary signal modelling via discrete-time TARMA (time-dependent autoregressive moving average) representations of the form

$$x_t + \phi_1(t)\cdot x_{t-1} + \cdots + \phi_n(t)\cdot x_{t-n} = w_t + \theta_1(t)\cdot w_{t-1} + \cdots + \theta_m(t)\cdot w_{t-m}$$

$$\Rightarrow \sum_{i=0}^{n} \phi_i(t)\cdot x_{t-i} = \sum_{i=0}^{m} \theta_i(t)\cdot w_{t-i}, \tag{7}$$

with $t = 0, 1, 2, \ldots$ henceforth indicating discrete time, x_t the sampled zero-mean non-stationary vibration signal modelled, w_t a stationary innovations (uncorrelated) signal with zero mean and variance σ_w^2, $\phi_i(t)$ $(i = 0, \ldots, n)$ the model's autoregressive (AR) parameters, and $\theta_i(t)$ $(i = 0, \ldots, m)$ the model's moving average (MA) parameters. Notice that $\phi_0(t) \equiv \theta_0(t) \equiv 1$, while the rest of the AR/MA parameters are assumed to belong to a functional subspace of dimensionality p, spanned by a set of linearly independent functions

$\{G_1(t), G_2(t), \ldots, G_p(t)\}$ (subspace basis functions): that is

$$\phi_i(t) \triangleq \sum_{j=1}^{p} a_{i,j} G_j(t), \qquad \theta_i(t) \triangleq \sum_{j=1}^{p} c_{i,j} G_j(t), \tag{8}$$

with $a_{i,j}$ and $c_{i,j}$ representing the AR and MA, respectively, coefficients of projection. The model defined by expressions (7) and (8) is referred to as a TARMA$(n, m)_p$ model, whereas that obtained by setting $\theta_i(t) \equiv 0$ $(i = 1, \ldots, m)$ is referred to as a pure TAR$(n)_p$ model [9, 10].

TAR/TARMA model estimation is performed by directly operating (in a "batch" mode) upon the complete designated signal record. Pure TAR estimation is based upon linear regression [10]. TARMA estimation is, on the other hand, significantly more complicated, and thus very rarely used. In order to alleviate its various complications, TARMA estimation is presently based upon the novel Polynomial-Algebraic (PA) method recently developed by the second author and his co-workers [10] and is followed by prediction error (PE) refinement. The PA method is effective in overcoming the difficulties associated with TARMA estimation, including the acute local extrema problems, the need for accurate initial guess parameter values, and that of high computational complexity. The PE stage aims at potential refinement of the attained parameter estimates. A brief account of TARMA parameter estimation is presented in Appendix A. A general procedure for subspace dimensionality, basis function, and model order selection is presented in section 3.2. Model validation is discussed in section 4.

Once a TARMA, or pure TAR, model has been estimated, its "frozen" time-dependent spectrum is obtained as:

$$S(\omega, t) = \left| \frac{\sum_{i=0}^{m} \theta_i(t)\, \mathrm{e}^{-\mathrm{j}\omega T_s i}}{\sum_{i=0}^{n} \phi_i(t)\, \mathrm{e}^{-\mathrm{j}\omega T_s i}} \right|^2 \cdot \sigma_w^2, \tag{9}$$

with ω representing frequency in rad/s, j the imaginary unit, $|\cdot|$ magnitude, and T_s the sampling period used ($T_s = 0{\cdot}08$ s).

3.2. TAR AND TARMA VIBRATION SIGNAL MODELLING

Following sample mean subtraction, the 2950 sample-long vibration signal is split into two disjoint sets: The $N_e = 2850$ sample ($\Delta T_e = 228$ s) long *estimation set* and the $N_v = 100$ sample ($\Delta T_v = 8$ s) long *validation set*. The former is used for model estimation, whereas the latter is, according to the cross-validation principle, exclusively reserved for model validation purposes.

Based upon the periodic nature of the non-stationary vibration signal, projections of the AR/MA parameters onto a subspace spanned by sine and cosine functions of the form

$$G_0(t) = 1, \qquad G_k(t) = \sin\left(\frac{k\pi}{N_e} t\right), \qquad \bar{G}_k(t) = \cos\left(\frac{k\pi}{N_e} t\right) \tag{10}$$

are sought. In the above expressions $k = 1,2, \ldots, N_e - 1$, whereas $t = 0, 1, 2, \ldots$ (discrete time).

TARMA/TAR subspace dimensionality, basis functions, and model orders are determined by the following three-step procedure. (a) In the first step, pure TAR models of fixed ("long") order and subspace dimensionality fixed to $p = 3$ [in order to incorporate $G_0(t)$ along with a pair of sine/cosine functions in their basis] are successively estimated. Based upon these results, the "best" potential basis functions (judged by the achieved model quality-of-fit) are selected and ranked. (b) In the second step, TAR models of fixed ("long") order but increasing subspace dimensionality are considered by sequentially adding to their subspace the best, second best, and so on, basis functions, until no significant improvement in model quality-of-fit is achieved. The adequate subspace dimensionality p and corresponding basis functions are thus determined. (c) In the third step pure TAR or mixed TARMA models of various orders, but with the predetermined subspace dimensionality and basis functions, are estimated until no improvement in the model quality-of-fit is achieved, and the required orders are thus determined. In this course the previously selected subspace dimensionality and basis functions may be also varied and contrasted against potential alternatives before a final selection is made.

Model quality-of-fit is, in the present context, judged in terms of the model residual sum of squares (RSS) (sum of the squares of the model-based one-step-ahead prediction errors) sometimes normalized by the (mean-corrected) series sum of squares (SSS), the model's multiple-step-ahead predictive ability, as well as Akaike's first and second information criteria (AIC and BIC respectively) [8].

The application of the above procedure, using $\mathrm{TAR}(28)_{p=3}$ models with $G_0(t)$ and a variety of other candidate functions, leads to $k = 228$ characterizing the best sine and cosine basis function pair. Quite expectedly, this corresponds to the exact system frequency of $f_p = 0{\cdot}5$ Hz (step (a)). Attempted subspace dimensionality increases lead to no improvement in the model quality-of-fit (step (b)).

The estimation of $\mathrm{TAR}(n)_{p=3}$ models with the foregoing subspace basis and of various orders does not lead to a concrete selection as the RSS is monotonically decreasing. The AIC follows a similar pattern, leading to very high orders ($n > 70$), while the BIC has strikingly different behaviour, favouring lower order models and suggesting the $\mathrm{TAR}(12)_{p=3}$ model as potentially adequate. The $\mathrm{TAR}(12)_{p=3}$ model, which is also characterized by a relatively reasonable parametrization, is thus selected as the best TAR model (partial modelling results in Table 2). It is interesting to note that this selection is supported by further analysis indicating the superior spectral accuracy of this model over higher order alternatives (step (c); TAR models).

The estimation (PA method) of mixed $\mathrm{TARMA}(n, m)_{p=3}$ models of various orders n, m ($n \geqslant 4$) leads to much more consistent results, as the RSS, AIC, and BIC criteria uniformly lead to a $\mathrm{TARMA}(4,5)_{p=3}$ model with a $\mathrm{TARMA}(4,3)_{p=3}$ representation suggested as second best (partial results in Figure 4). This selection is quite reasonable as the underlying system is of fourth order and the torque excitation uncorrelated. Prediction-error-based model refinement (initialized with

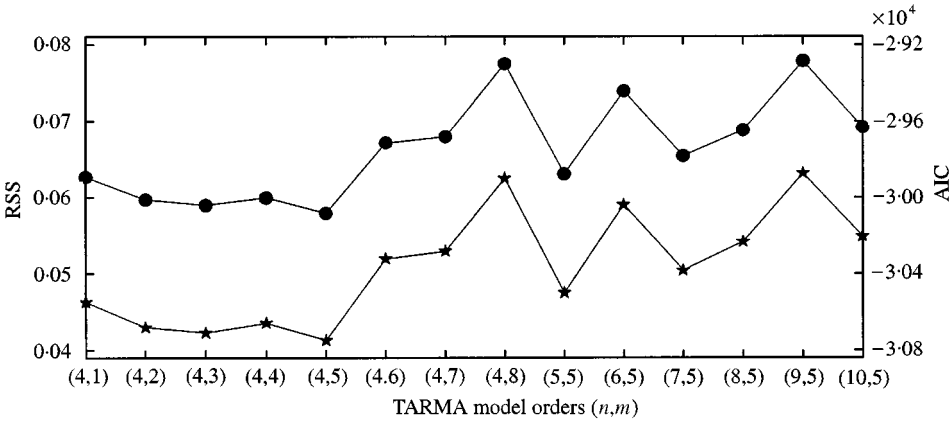

Figure 4. RSS (—●—) and AIC (—★—) of various TARMA models (estimation set; PA method).

TABLE 2

Comparison of the estimated $\mathrm{TAR}(12)_{p=3}$, $\mathrm{PA\text{-}TARMA}(4,3)_{p=3}$, $\mathrm{PA\text{-}TARMA}(4,5)_{p=3}$, *and* $\mathrm{PE\text{-}TARMA}(4,5)_{p=3}$ *models in terms of* RSS, RSS/SSS, AIC, BIC (*estimation set*), *parametric complexity*, *as well as achieved prediction accuracy* (*validation set*) [*minimal values in bold face characters*]

	$\mathrm{TAR}(12)_{p=3}$	$\mathrm{PA\text{-}TARMA}(4,3)_{p=3}$	$\mathrm{PA\text{-}TARMA}(4,5)_{p=3}$	$\mathrm{PE\text{-}TARMA}(4,5)_{p=3}$
RSS	0·05491	0·05716	0·05643	**0·04960**
RSS/SSS	3·22%	3·35%	3·31%	**2·91**%
AIC	− 30,881·63	− 30,797·22	− 30,821·72	− **31,189·41**
BIC	− 25,167·19	− 25,173·75	− 25,161·12	− **25,525·21**
Par. complexity	36	**21**	27	27
	Prediction error† (%)			
1-step	**2·855**	3·345	3·196	3·031
5-step	**4·906**	5·538	5·148	4·918
8-step	5·534	5·944	5·904	**5·454**

† Prediction error is expressed as a percentage of the signal full scale (max minus min values).

the PA estimates) is subsequently found to lead to further improvement in the $\mathrm{TARMA}(4,5)_{p=3}$ case, but to no improvement in the $\mathrm{TARMA}(4,3)_{p=3}$ case. The final TARMA modeling results, including the $\mathrm{PA\text{-}TARMA}(4,3)_{p=3}$, $\mathrm{PA\text{-}TARMA}(4,5)_{p=3}$ and $\mathrm{PE\text{-}TARMA}(4,5)_{p=3}$ models, are summarized in Table 2. From these it is evident that the $\mathrm{PE\text{-}TARMA}(4,5)_{p=3}$ model is (based upon the RSS, AIC and BIC criteria) superior to all alternative TARMA representations,

TABLE 3

The estimated PE-TARMA$(4,5)_{p=3}$ *model coefficients of projection* $[G_1(t) = 1, G_2(t) = \cos(228\pi t/N_e), G_3(t) = \sin(228\pi t/N_e)$; $s = 15, b = 5$ *in the PA method*]

AR coefficients				MA coefficients			
	$j=1$	$j=2$	$j=3$		$j=1$	$j=2$	$j=3$
$a_{1,j}$	−1·2748	0·0548	−0·2001	$c_{1,j}$	0·0932	0·0575	−0·0440
$a_{2,j}$	0·8583	−0·1519	0·3147	$c_{2,j}$	−0·4571	−0·0136	−0·0333
$a_{3,j}$	−0·9329	0·1892	−0·1501	$c_{3,j}$	0·2022	0·0807	0·0368
$a_{4,j}$	0·7968	−0·0831	−0·0379	$c_{4,j}$	−0·1491	−0·0065	−0·0101
				$c_{5,j}$	0·0902	−0·1028	−0·0274

and is thus selected as best. The estimated PE-TARMA$(4,5)_{p=3}$ model parameters are presented in Table 3 (step (c), TARMA models).

4. MODEL ANALYSIS AND DISCUSSION

Model validation: The TAR$(12)_{p=3}$ and PE-TARMA$(4,5)_{p=3}$ models are successfully validated by assessing residual whiteness at the $\alpha = 0{\cdot}05$ level (probability of error 0·05) within the validation set. Model-based one-step-ahead predictions are, for the PE-TARMA$(4,5)_{p=3}$ case and within the validation set, presented in Figure 5. It is important to observe that the predictions follow the signal with remarkable accuracy, with the actual signal values falling well within their estimated 95% probability limits.

Model fit criteria: Comparing the selected PE-TARMA$(4,5)_{p=3}$ model with the "long" TAR$(12)_{p=3}$ model is also of interest. The results in Table 2 indicate that the PE-TARMA$(4,5)_{p=3}$ model clearly surpasses its TAR$(12)_{p=3}$ counterpart in terms of the RSS, AIC, and BIC criteria, while additionally offering a more parsimonious representation (reduced parametric complexity). The TAR$(12)_{p=3}$ model succeeds in achieving slightly improved prediction accuracy within the validation set for the indicated 1- and 5-step-ahead horizons, whereas the PE-TARMA$(4,5)_{p=3}$ model prevails at longer, such as the indicated 8-step-ahead, horizons.

Time-dependent spectrum: The time-dependent spectrum is an important and particularly useful outcome of the analysis. The estimated PE-TARMA$(4,5)_{p=3}$ model-based "frozen" time-dependent spectrum is shown (in both 3-D and contour plots) in Figure 6 as a function of time and frequency. It is observed that this is in remarkably close agreement with the theoretical (continuous-time) signal spectrum (Figure 2), exhibiting high accuracy, resolution and tracking. As is usually the case with stationary signals, the spectral agreement is superior for the two time-dependent spectral peaks, while also being sufficiently accurate for the valley.

The estimated TAR$(12)_{p=3}$ model-based spectrum is shown in Figure 7. It is readily observed that while the first spectral peak [$f_1(t)$ in the 0·84 − 0·92 Hz range] is estimated accurately, the second one [$f_2(t)$, theoretically in the

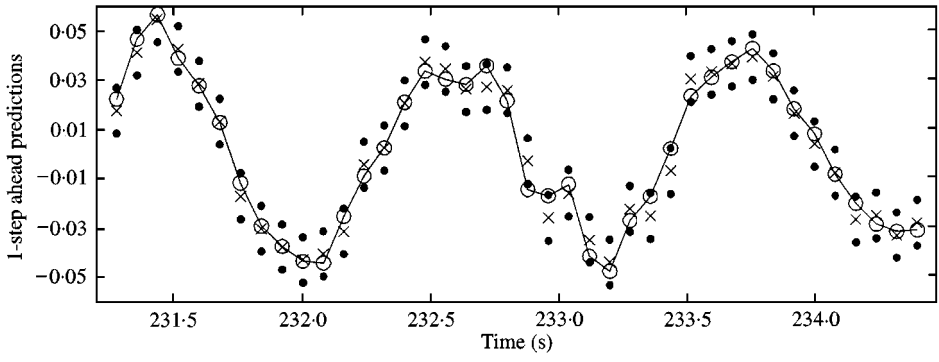

Figure 5. PE-TARMA(4,5)$_{p=3}$ model-based one-step-ahead predictions within the validation set (○: actual signal, ×: predictions, ●: 95% probability limits).

3·48–3·90 Hz range] is somewhat levelled off. Moreover, additional (false) peaks are in this case introduced in the 2–3 Hz range, and also in the neighbourhood of 5 Hz (the former being more evident on the contour plot).

For purposes of comparison, a non-parametric, Blackman–Tukey type, Fourier-based estimate of the time-dependent spectrum is also obtained. Toward this end an estimate of the non-stationary autocorrelation function within a single system period is (using the system periodicity of $N_p = 25$ samples) computed as

$$\hat{R}_{xx}(i, i+\tau) = \frac{1}{P-2} \sum_{n=1}^{P-2} x_{i+nN_p} \cdot x_{i+nN_p+\tau}, \quad i = 0, 1, 2, \ldots, N_p - 1. \tag{11}$$

In this expression, i indicates discrete time within a system period, n the integer number of system periods which constitute past at the present discrete time t ($n = 0, 1, 2, \ldots, P-1$, with $P = 114$ designating the total number of system periods included in the estimation set). Using this notation the discrete absolute time t ($t = 0, 1, 2, \ldots, N_e - 1$) is expressed as

$$t = i + nN_p,$$

while τ represents lag ($\tau = 0, \pm 1, \pm 2, \ldots, \tau_{\max}$, with $\tau_{\max} = 25$). Estimator (11) thus provides the non-stationary autocorrelation function by treating each $N_p = 25$ sample-long segment as a different realization, and subsequently averaging over the $P-2$ such realizations used [notice that the first and last segments are not used in equation (11)]. Once $\hat{R}_{xx}(i, i+\tau)$ is available, the time-dependent spectrum estimate is obtained as the Fourier transform

$$S(\omega, t) = \sum_{\tau=-\tau_{\max}}^{\tau_{\max}} \hat{R}_{xx}(i, i+\tau) \cdot w(\tau) \cdot \mathrm{e}^{-j\omega T_s \tau}, \tag{12}$$

with $w(\tau)$ designating a proper lag window (a symmetric Hamming window is presently used). The magnitude of the obtained non-parametric time-dependent

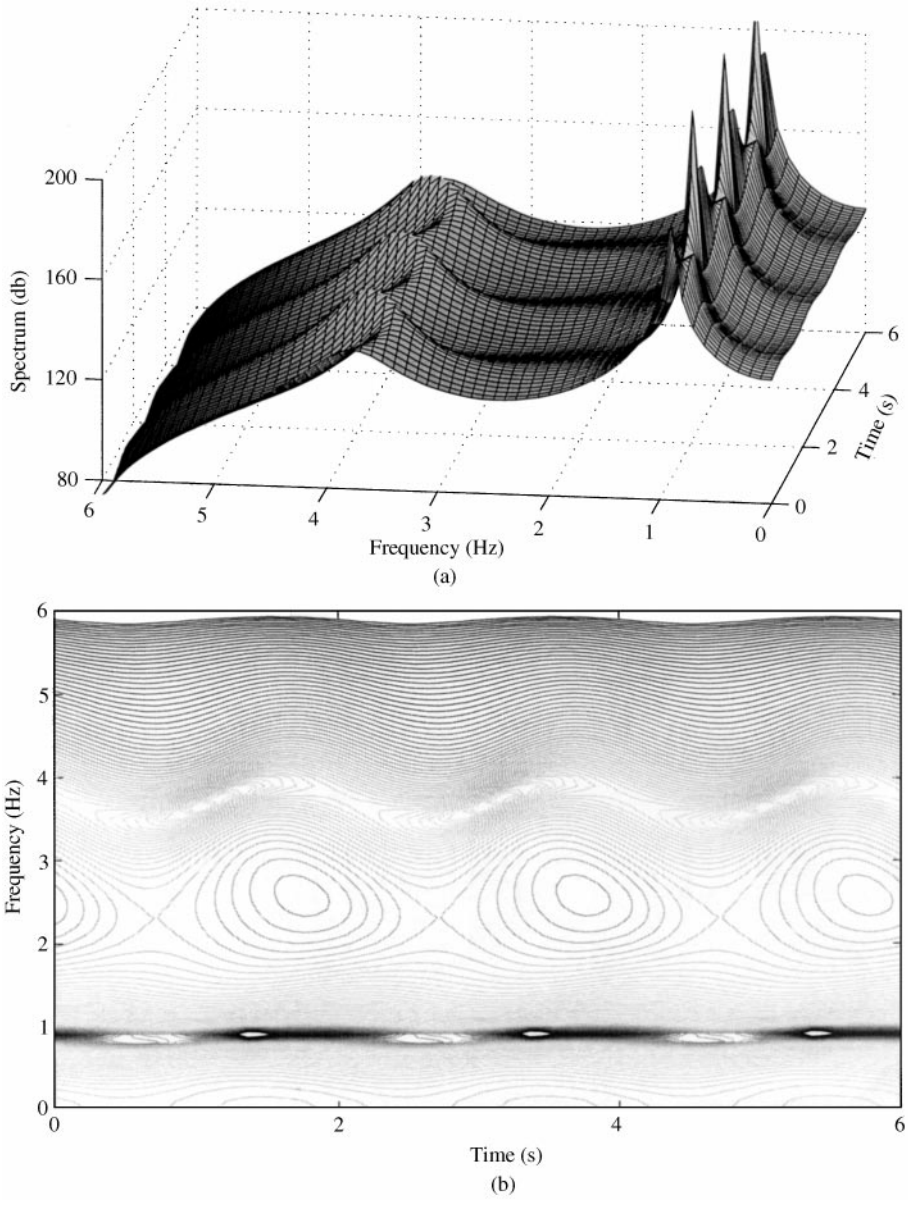

Figure 6. Time-dependent spectrum of the PE-TARMA(4,5)$_{p=3}$ signal model. (a) 3-D plot; (b) contour plot.

spectrum estimate is depicted in Figure 8 (note that for purposes of consistency and direct comparison with the parametric spectra, the non-parametric spectrum is repeated over three system periods). The two spectral peaks $f_1(t)$ and $f_2(t)$ may be still seen; the first one being more evident and the second quite rough. In both cases, however, frequency tracking, as well as spectral accuracy and resolution, are inadequate, and nowhere close to those obtained by the parametric functional series [TARMA(4,5)$_{p=3}$ or TAR(12)$_{p=3}$] models. This behaviour is typical of non-parametric methods and highlights some of the important advantages that

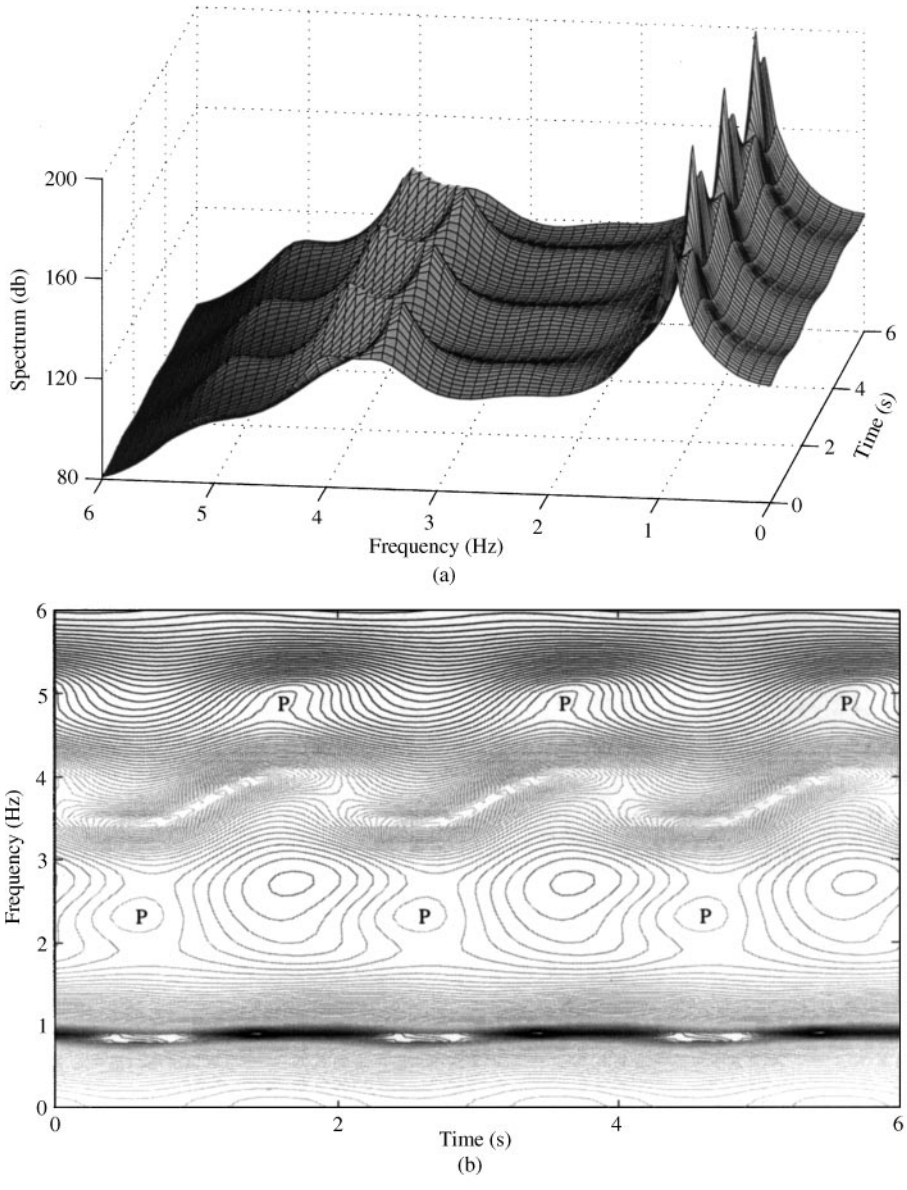

Figure 7. Time-dependent spectrum of the $\mathrm{TAR}(12)_{p=3}$ signal model. (a) 3-D plot; (b) contour plot (false peaks are indicated by "p").

a parametric — and in particular the TARMA — functional series method may offer.

Modal parameters: Further insight into the achieved estimation accuracy may be obtained by comparing the physically significant estimated time-dependent "frozen" modal parameters [natural frequencies $f_1(t)$, $f_2(t)$ and damping ratios $\zeta_1(t), \zeta_2(t)$] to their theoretical counterparts. The $\mathrm{TARMA}(4,5)_{p=3}$ modal parameters are presented in Figure 9, from which the agreement between the

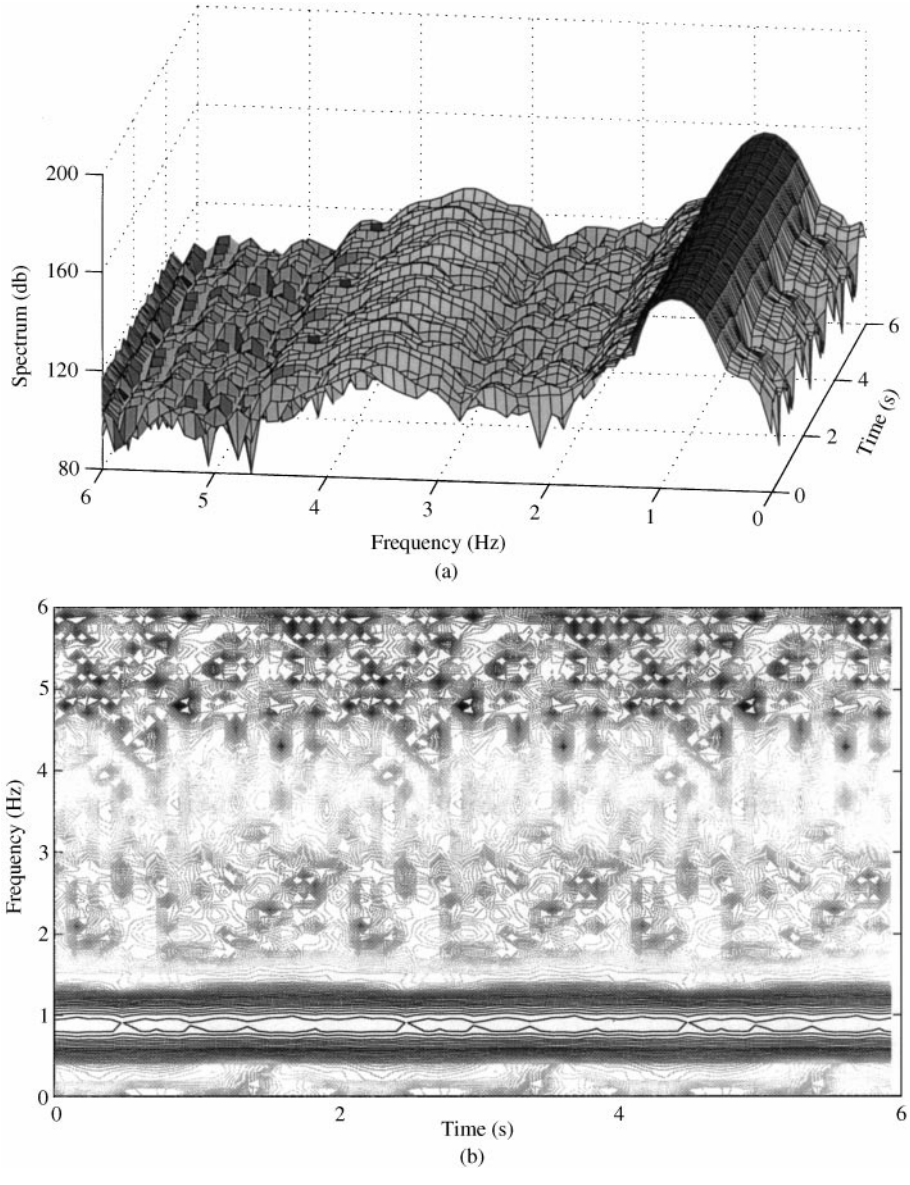

Figure 8. Non-parametric Fourier-based time-dependent spectrum of the signal. (a) 3-D plot; (b) contour plot.

respective natural frequency trajectories is quite good, and so is that of the respective damping ratios (notice the small values of the latter that pose serious estimation accuracy problems [13]).

The estimated $\text{TAR}(12)_{p=3}$ model is, on the other hand, substantially oversized, characterized by six pairs of time-varying "frozen" complex poles, with each one giving rise to a corresponding mode of vibration. The first $\text{TAR}(12)_{p=3}$ mode corresponds to the first mode $[f_1(t), \zeta_1(t)]$ of the actual system, and the estimates are not very different from those obtained by the $\text{TARMA}(4,5)_{p=3}$ model. The

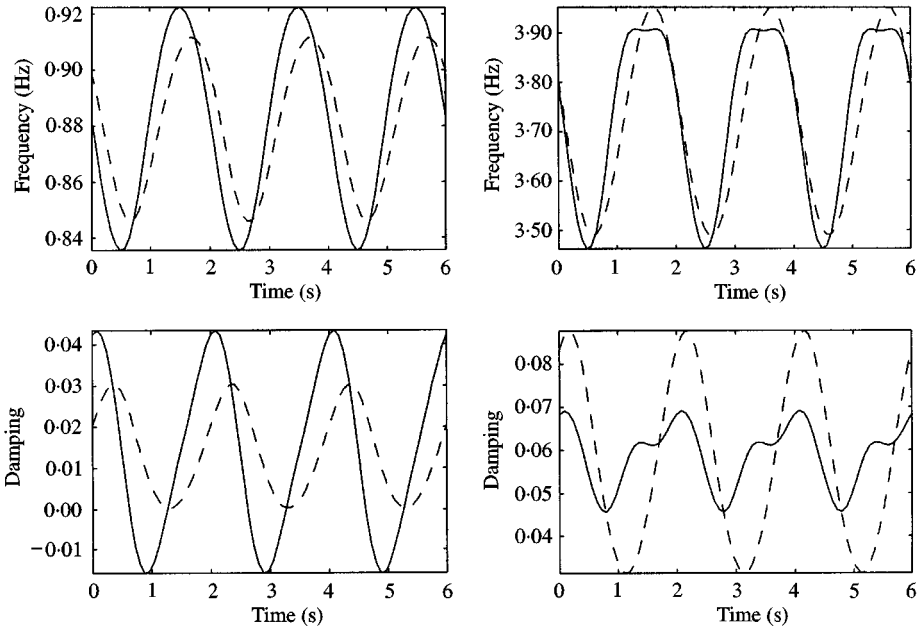

Figure 9. Time-varying natural frequencies and damping ratios of the vibration signal [——: theoretical, – – –: PE-TARMA(4,5)$_{p=3}$ based].

second mode corresponds to a (false) natural frequency in the 1·00–1·40 Hz range [$\zeta(t)$ in the 0·47–0·80 range], while the third one corresponds also to the false frequency observed in the spectrum (Figure 7) in the 2–3 Hz range [$\zeta(t)$ in the 0·18–0·30 range]. The fourth and fifth modes *both* cover the frequency range of the second system mode [$f_2(t), \zeta_2(t)$], but at significantly reduced accuracy. The presence of two modes in this range explains the levelling off already observed in the TAR(12)$_{p=3}$ spectrum. The sixth mode finally corresponds to the second false frequency observed in the spectrum (Figure 7) in the neighbourhood of 5 Hz [$\zeta(t)$ in the 0·06–0·11 range].

Evidently, the estimation of the time-varying system modal parameters is accurately achieved through TARMA analysis, while being very difficult to achieve through TAR analysis. The latter not only lacks in terms of achievable accuracy, but it also provides a number of false additional modes which are practically difficult to identify as such. The capability of providing unambiguous and accurate estimates of the physically meaningful modal parameter trajectories constitutes an important asset of mixed TARMA analysis, and is a reflection of the much more direct relationship of a mixed TARMA model with the underlying physical system.

5. CONCLUDING REMARKS

The problem of non-stationary vibration modelling and analysis was studied through a manipulator vibration paradigm. Parametric Functional Series TARMA analysis was applied for the first time within the vibration analysis context, and comparisons with both pure TAR and non-parametric Fourier-based analysis were

made. These focussed on achievable time-dependent spectrum accuracy, resolution, tracking, as well as on estimated modal parameter accuracy.

The study confirmed the applicability, effectiveness, and important advantages of the Functional Series TARMA method for non-stationary signal modelling and analysis. The method is suitable for exploring non-stationarity in a broad range of problems, as a wide variety of non-stationary vibration signals may be modelled via proper functional basis selection. A recent example is earthquake strong ground motion where Haar wavelet functional bases are used [14].

Some of the specific conclusions of this study are as follows,

1. The Functional Series TAR/TARMA approach led to signal representations which are meaningfully characterized by basis functions that include a constant and a sine/cosine pair featuring the exact system frequency of $f_p = 0{\cdot}5$ Hz.
2. The TARMA method unambiguously led to a physically meaningful non-stationary TARMA$(4,5)_{p=3}$ representation. The pure TAR method did not lead to a definite selection due to contradictory behaviour of the RSS, AIC and BIC criteria. Nevertheless, a TAR$(12)_{p=3}$ model was eventually selected as best.
3. The estimated TARMA$(4,5)_{p=3}$ model was shown to surpass its TAR$(12)_{p=3}$ counterpart in terms of the RSS, AIC, and BIC criteria. It was also shown to be characterized by a lower parametrization and a more direct relationship with the underlying physical system, thus being both physically meaningful and advantageous to use in analysis, prediction and control.
4. The TARMA$(4,5)_{p=3}$-based time-dependent spectrum was shown to exhibit superior accuracy, resolution, and tracking. Although capturing the main signal features, the corresponding TAR$(12)_{p=3}$ spectrum was shown to exhibit false additional peaks. The non-parametric Fourier-based spectrum was shown to be of inferior quality, demonstrating some of the difficulties of non-parametric time-varying spectrum estimation. In this study these were additionally due to the fact that spectral estimation had to be based upon only $N_p = 25$ samples per system period.
5. The TARMA$(4,5)_{p=3}$-based time-dependent modal parameters (natural frequencies and damping ratios) were shown to be in good overall agreement with their theoretical counterparts. This was, however, not the case with the TAR$(12)_{p=3}$-based modal parameters, which were both less accurate and ambiguous, as they were mixed with those of the false modes and their distinction was difficult. The capability of providing unambiguous and accurate estimates of the physically meaningful modal parameter trajectories is a result of the direct relationship of the estimated TARMA model with the underlying physical system, and constitutes an important asset of the mixed TARMA method.

REFERENCES

1. L. Cohen 1995 *Time-Frequency Analysis*. Englewood Cliffs, NJ: Prentice-Hall PTR.

2. J. K. Hammond and P. R. White 1996 *Journal of Sound and Vibration* **190**, 419–447. The analysis of non-stationary signals using time–frequency methods.
3. M. B. Priestley 1989 *Nonlinear and Nonstationary Time Series Analysis*. London: Academic Press.
4. D. E. Newland 1993 *Random Vibrations, Spectral and Wavelet Analysis*. London: Addison–Wesley, Longman, third edition.
5. D. E. Newland 1994 *Journal of Vibration and Acoustics* **116**, 409–425. Wavelet analysis of vibration, Parts 1 and 2.
6. M. G. Bellanger 1987 *Adaptive Filters and Signal Analysis*. New York: Marcel Dekker.
7. Q. Zhuge, Y. Lu and S. Yang 1990 *Mechanical Systems and Signal Processing* **4**, 355–365. Non-stationary modelling of vibration signals for monitoring the condition of machinery.
8. G. Kitagawa and W. Gersch 1996 *Smoothness Priors Analysis of Time Series*. New York: Springer-Verlag.
9. Y. Grenier 1989 *Time and Frequency Representation of Signals and Systems* (G. Longo and B. Picinbono, editors). New York: Springer-Verlag. Parametric time–frequency representations.
10. R. Ben Mrad, S. D. Fassois and J. A. Levitt 1998 *Signal Processing* **65**, 1–19. A polynomial-algebraic method for non-stationary TARMA signal analysis, Part I: the method.
11. G. N. Fouskitakis, J. S. Sakellariou and S. D. Fassois 1998 *Proceedings of the 5th National Congress on Mechanics, Ioannina, Greece*, 742–749. Non-stationary stochastic modeling and simulation of strong earthquake ground motion: an exploratory study.
12. G. Jumarie 1996 *Journal of Intelligent and Robotic Systems* **16**, 245–267. Tracking control of manipulators with active inertias by using sliding Lagrangian.
13. S. D. Fassois, K. F. Eman and S. M. Wu 1990 *Journal of Dynamic Systems, Measurement and Control* **112**, 1–9. Sensitivity analysis of the discrete-to-continuous dynamic system transformation.
14. G. N. Fouskitakis and S. D. Fassois 1999 *Report Series on Stochastic Mechanical Systems* 99-02, *University of Patras*. Non-stationary functional series TARMA modeling of strong earthquake ground motion (also submitted for journal publication).
15. E. W. Kamen 1988 *Linear Algebra and Its Applications* **98**, 263–289. The poles and zeros of a linear time-varying system.
16. J. E. Dennis and R. B. Schnabel 1983 *Numerical Methods for Unconstrained Optimization and Nonlinear Equations*. Englewood Cliffs, NJ: Prentice-Hall Inc.

APPENDIX A: FUNCTIONAL SERIES TARMA MODEL ESTIMATION

The TARMA representation (7) may be compactly re-written as

$$A(B, t)\, x_t = C(B, t)\, w_t, \tag{A1}$$

with

$$A(B, t) \triangleq 1 + \phi_1(t)\, B + \cdots + \phi_n(t)\, B^n, \qquad C(B, t) \triangleq 1 + \theta_1(t)\, B + \cdots + \theta_m(t)\, B^m \tag{A2}$$

representing the time-dependent autoregressive (AR) and moving average (MA) polynomials expressed in terms of the backshift operator $B(Bx_t \triangleq x_{t-1})$. In the above it is assumed that $\phi_n(t) \neq 0$ and $\theta_m(t) \neq 0$ for at least some t.

TARMA estimation is based upon the Polynomial-Algebraic (PA) method followed by Prediction Error (PE)-based potential model refinement.

A.1. POLYNOMIAL-ALGEBRAIC (PA) ESTIMATION

The Polynomial-Algebraic (PA) method is based upon a non-commutative B polynomial operator algebra defined by the usual addition and the "*skew*" *multiplication operation* "$\circ$" [15]:

$$B^i \circ B^j = B^{i+j}, \qquad B^i \circ x_t = x_{t-i} B^i \quad \forall x_t. \tag{A3}$$

A concise overview of the stages of the method is as follows (the interested reader is referred to Reference [10] for further details).

Stage 1: *Inverse function estimation.*

Consider an inverse function model of the form

$$I(B, t)\, x_t = e_t^{ar}, \tag{A4}$$

with the time-dependent inverse polynomial operator $I(B, t)$ being theoretically defined as

$$I(B, t) \triangleq 1 + I_1(t)\, B + I_2(t)\, B^2 + \cdots \triangleq C^{-1}(B, t) \circ A(B, t), \tag{A5}$$

while x_t, e_t^{ar} designate the signal modelled and the model's one-step-ahead prediction error, respectively. Expanding each one of the $I_i(t)$ functions in terms of the basis functions, and truncating model (A4) to a finite (s) order leads to the approximate representation

$$x_t \approx -[\mathbf{m}_{t-1,t}^{\mathrm{T}} \mathbf{m}_{t-2,t}^{\mathrm{T}} \cdots \mathbf{m}_{t-s,t}^{\mathrm{T}}]\, \boldsymbol{\xi} + \mathrm{e}_t^{ar}, \tag{A6}$$

with the vector $\mathbf{m}_{t-i,t}[p \times 1]$ defined as

$$\mathbf{m}_{t-i,t} \triangleq [G_1(t)\, G_2(t) \cdots G_p(t)]^{\mathrm{T}}\, x_{t-i}, \quad 1 \leqslant i \leqslant s,$$

and $\boldsymbol{\xi}[ps \times 1]$ representing the inverse operator coefficient of projection vector

$$\boldsymbol{\xi} \triangleq [I_{1,1}\, I_{1,2} \ldots I_{1,p} \vdots I_{2,1}\, I_{2,2} \ldots I_{2,p} \vdots \ldots \vdots I_{s,1}\, I_{s,2} \ldots I_{s,p}]^{\mathrm{T}}.$$

Minimization of a quadratic form of the prediction error $\{e_t^{ar}\}$ leads to the linear regression estimator

$$\hat{\boldsymbol{\xi}} = -\left(\sum_{t=t_0+s}^{t_f} [\mathbf{m}_{t-1,t} \ldots \mathbf{m}_{t-s,t}^{\mathrm{T}}]^{\mathrm{T}} [\mathbf{m}_{t-1,t}^{\mathrm{T}} \cdots \mathbf{m}_{t-s,t}^{\mathrm{T}}] \right)^{-1}$$
$$\cdot \left(\sum_{t=t_0+s}^{t_f} [\mathbf{m}_{t-1,t}^{\mathrm{T}} \cdots \mathbf{m}_{t-s,t}^{\mathrm{T}}]^{\mathrm{T}}\, x_t \right) \tag{A7}$$

in which t_o, t_f represent the signal's initial and final observation times, respectively.

Stage 2: *Initial AR/MA estimation*

The inverse polynomial operator definition (A5) leads to

$$\theta_i(t) = \phi_i(t) - I_i(t) - \sum_{j=1}^{i-1} \theta_j(t)\, I_{i-j}(t-j). \tag{A8}$$

Substituting the functional expansions of the AR, MA, and inverse polynomial operators into equation (A8) leads to the expression

$$c_{i,k} = a_{i,k} - I_{i,k} - \sum_{j=1}^{i-1} \sum_{q=1}^{p} \sum_{r=1}^{p} c_{j,q}\, I_{i-j,r} S_{q,r}^{j,k}, \quad 1 \leqslant k \leqslant p, \tag{A9}$$

with the quantities $S_{q,r}^{j,k}$ designating the projections of the product $G_q(t)\, G_r(t-j)$ onto the subspace spanned by the functions $\{G_1(t), G_2(t), \ldots, G_p(t)\}$.

MA estimation is then based upon substitution of the previously obtained inverse operator estimates $\hat{I}_{i,k}$ into expressions (A9) and the solution of the resulting, for $i = \max(n, m) + 1, \ldots, \max(n, m) + m$, linear system of equations

$$\sum_{j=1}^{m} \sum_{q=1}^{p} \sum_{r=1}^{p} c_{j,q} I_{i-j,r} S_{q,r}^{j,k} = -I_{i,k} \quad (\max(n, m) + 1 \leqslant i \leqslant \max(n, m) + m;$$
$$1 \leqslant k \leqslant p) \tag{A10}$$

Corresponding AR parameter estimates are subsequently obtained by solving the set of equations (A9) for $i = 1, \ldots, n$, following the replacement of the MA parameters by their obtained estimates.

Stage 3: *β Polynomial operator estimation*

A $\beta(B, t)$ polynomial operator of the form $\beta(B, t) \triangleq 1 + \sum_{i=1}^{\infty} \beta_i(t)\, B^i$ is defined through the identity

$$I(B, t) \triangleq C^{-1}(B, t) \circ A(B, t) \triangleq A(B, t) \circ \beta(B, t) \tag{A11}$$

which leads to

$$\beta_i(t) = I_i(t) - \phi_i(t) - \sum_{j=1}^{i-1} \phi_j(t)\, \beta_{i-j}(t-j). \tag{A12}$$

Expanding each one of the $\beta_i(t)$ functions in terms of the basis functions $\{G_1(t), G_2(t), \ldots, G_p(t)\}$ and using the corresponding expansions of the inverse, AR and MA operators leads to

$$\beta_{i,k} = I_{i,k} - a_{i,k} - \sum_{j=1}^{i-1} \sum_{q=1}^{p} \sum_{r=1}^{p} a_{j,q} b_{i-j,r} S_{q,r}^{j,k} \qquad 1 \leqslant k \leqslant p. \tag{A13}$$

Given estimates of the inverse function and AR coefficients of projection, the first v (for $i = 1, 2, \ldots, v$) of expressions (A13) may be solved for the coefficients of projection $\beta_{i,k}$ ($i = 1, 2, \ldots, v$; $k = 1, 2, \ldots, p$) of a finite, vth order, approximation of $\beta(B, t)$.

Stage 4: *AR parameter estimation*

Upon assuming small changes in the estimates obtained in two successive iterations, say r and $r - 1$, the TARMA model at iteration r may be approximated as

$$\mathrm{e}_t^r \approx [A^r(B, t) \circ \beta^{r-1}(B, t)]\, x_t = A^r(B, t)\, \bar{x}_t^r, \tag{A14}$$

with the superscript denoting the iteration in which the indicated polynomial is estimated and $\{\bar{x}_t^r\}$ the filtered sequence

$$\bar{x}_t^r \triangleq \beta^{r-1}(B, t)\, x_t. \tag{A15}$$

Model (A14) is re-written as

$$\bar{x}_t^r = -\,[\bar{\mathbf{m}}_{t-1,t}^{\mathrm{T}} \ldots \bar{\mathbf{m}}_{t-n,t}^{\mathrm{T}}]\, \boldsymbol{\phi}^r + \mathrm{e}_t^r, \tag{A16}$$

with $\boldsymbol{\phi}^r$ representing the AR parameter vector (parameterized in terms of the corresponding coefficients of projection)

$$\boldsymbol{\phi}^r \triangleq [a_{1,1}^r\ a_{1,2}^r \ldots a_{1,p}^r \vdots\ a_{2,1}^r\ a_{2,2}^r\ \cdots a_{2,p}^r \vdots \ldots \vdots\ a_{n,1}^r\ a_{n,2}^r\ \ldots a_{n,p}^r]^{\mathrm{T}} \quad [np \times 1]$$

and

$$\bar{\mathbf{m}}_{t-i,t} \triangleq [G_1(t)\, G_2(t) \ldots G_p(t)]^{\mathrm{T}}\, \bar{x}_{t-i}^r \quad (1 \leqslant i \leqslant n) \quad [p \times 1].$$

Minimization of a quadratic form of the prediction error $\{e_t^r\}$ leads, in the rth iteration, to the linear regression estimator

$$\hat{\boldsymbol{\phi}}^r = \left(\sum_{t=t_o+n}^{t_f} [\bar{\mathbf{m}}_{t-1,t}^{\mathrm{T}} \ldots \bar{\mathbf{m}}_{t-n,t}^{\mathrm{T}}]^{\mathrm{T}}\, [\bar{\mathbf{m}}_{t-1,t}^{\mathrm{T}} \ldots \bar{\mathbf{m}}_{t-n,t}^{\mathrm{T}}] \right)^{-1} \cdot \left(\sum_{t=t_o+n}^{t_f} [\bar{\mathbf{m}}_{t-1,t}^{\mathrm{T}} \ldots \bar{\mathbf{m}}_{t-n,t}^{\mathrm{T}}]^{\mathrm{T}}\, \bar{x}_t^r \right). \tag{A17}$$

Stage 5: *MA parameter estimation*

MA parameter estimation is based upon expressions (A9), which, after replacing the AR and inverse function parameters by their respective estimates, form a linear system of equations with a uniquely determined solution.

A.2. PREDICTION ERROR (PE) ESTIMATION

Prediction error (PE) estimation is based upon minimization of a quadratic criterion of the form

$$J = \sum_{t=0}^{N_e-1} e_t^2 \tag{A18}$$

with $e_t \triangleq x_t - \hat{x}_{t/t-1}$ representing the TARMA model's (A1) one-step-ahead prediction error at time t. Criterion (A18) is non-quadratic with respect to the parameters to be estimated and frequently characterized by local extrema. Furthermore, its optimization is characterized by high computational complexity. To overcome these difficulties, the optimization, which is presently based upon a Levenberg–Marquardt scheme [16] with mixed quadratic and cubic line search, is initiated with the PA parameter estimates.

A.3. REMARKS

1. It is important to note that the PA method is based on exclusively linear operations and is thus characterized by computational simplicity, no local extrema problems, and no need for initial guess parameter values.
2. The orders s and v (Stages 1 and 3, respectively, of the PA method) should be selected sufficiently long. A useful rule of thumb is to try to select them in the range $(2 \cdots 8) \cdot \max(n, m)$, although somewhat higher values may be necessary for "low" order models.
3. Stages 3–5 of the PA method may be iterated until either acceptable convergence in the estimated parameters, or a minimum of the criterion (A18), is attained.